■動向

State of the Art in High Resolution Synchrotron Radiation Angle-Resolved Photoemission Spectroscopy

Moritz Hoesch,[1] Timur K. Kim,[1] Pavel Dudin[1] and Felix Baumberger[2]
[1]Diamond Light Source, Harwell Campus, Didcot OX11 0DE, United Kingdom
[2]Department of Quantum Matter Physics, University of Geneva, 24 Quai Ernest-Ansermet, 1211 Geneva 4, Switzerland and Swiss Light Source, Paul Scherrer Institut, 5232 Villigen PSI, Switzerland

A beamline for high resolution Angle-Resolved Photoemission Spectroscopy (ARPES) has been constructed at Diamond Light Source. The objective of the project was to provide a facility for the analysis of the electronic structures of solids and their surfaces. This article descibes the concepts chosen for the implementation of this objective, from the undulator source in the 3 GeV storage ring over the plane grating monochromator to the high-resolution ARPES end station and its in-situ sample preparation facilities. The beamline and its installations are proving highly productive and are thus considered the current state-of-the art in high-resolution ARPES.

I. INTRODUCTION

High resolution Angle-Resolved Photoemission Spectroscopy (ARPES) using synchrotron radiation is a mature technique, providing access to the momentum resolved spectral function of a broad range of materials. It is applied to the study of valence electron states of semiconductors and quasiparticle excitations near the Fermi surface of metals and superconductors. While in these systems, the surface is merely the access route to the bulk, ARPES is also used to investigate a wealth of artificially produced atomic structures on surfaces[1–3]. The surface sensitivity of ARPES arises from the short inelastic mean free path of the photoelectrons at kinetic energies low enough to allow for a very high energy resolution. In this article we focus on the range of $h\nu = 18$–240 eV, where the photon energy $h\nu$ is large compared to the the work function Φ of the samples under study.

The term high resolution itself undergoes continuous redefinitions to mean smaller and smaller numbers of the combined energy resolution ΔE_{comb}, which contains contributions from photon delivery ($\Delta E_{h\nu}$), electron spectrometer (ΔE_{ana}) and sample grounding and related effects (ΔE_{etc}). With suitable approximations, the combined resolution can be estimated as

$$\Delta E_{\mathrm{comb}} = \sqrt{(\Delta E_{h\nu})^2 + (\Delta E_{\mathrm{ana}})^2 + (\Delta E_{\mathrm{etc}})^2}. \quad (1)$$

In a properly designed instrument the third term ΔE_{etc} can often be neglected while a trade off between resolution and flux is used in both the photon beam ($\Delta E_{h\nu}$) and the electron analyser (ΔE_{ana}).

For the photon beam energy resolution $\Delta E_{h\nu}$ the synchrotron source does not have a natural advantage since the source requires monochromatisation. Laser and gas emission sources may have natural line widths that are more suitable to high resolution on their own already[4,5] and a monochromator is only needed to suppress unwanted photon lines. In the case of an undulator source in a synchrotron storage ring, the relative natural line width is the inverse of the number of undulator periods, usually less than 40. The monochromatisation is then performed in a grating monochromator with a typical resolving power $h\nu/\Delta E_{h\nu} \approx 20{,}000$. Furthermore the pulsed nature of the synchrotron beam with duty cycles of a few percent may lead to space charge effects that give rise to an intrinsic effective ultimate energy resolution and ultimate uncertainty in the calibration of the binding energy scale of electrons[6,7].

The key advantages of synchrotron radiation lie in the freely tuneable photon energy over a large range, the availability of polarised light, often freely selectable as well, and the very high flux in a small ultimate beam spot on the sample. This high flux enables the use of high resolution modes of the electron analyser at $\Delta E_{\mathrm{ana}} \leq 2$ meV and thus a $\Delta E_{\mathrm{tot}} \simeq 2$–$3$ meV under realistic data acquisition conditions.

Also all other aspects of the instrumentation are continuously evolving, and new ways of interpreting the rich data are leading to a refined understanding of what information can be obtained. Nevertheless, by-and-large the technique is well established. ARPES has proven such a successful

technique, giving a wealth of information about the ground state as well as the excitations of electrons in crystalline metals and semiconductors, that almost every synchrotron radiation source in the world has a station for ARPES in its beamline portfolio and new beamlines are constantly in the planning or implementation stage at some or the other source.

This article describes the design choices and implementation of a VUV to soft x-ray beamline and high resolution ARPES station at Diamond Light Source. The beamline features two branches, HR-ARPES and nano-ARPES and this paper focusses on the former and its end station. The paper is organised as follows. Sections II and III discuss the key performance parameters for beam delivery and end station, respectively, and discusses how these were decided. Sectio IV describes the sample preparation and characterisation facilities, and the final sections summarise the achieved performance and attempt an outlook into the near future of evolution of the field.

II. CHOICES FOR BEAM DELIVERY

The first choice to be made when designing an electron spectroscopy beamline is the range of photon energies to be covered. We consider five arguments for the choice of photon energy.

The photoemission process maps the occupied states in the material under investigation onto the intensity spectrum $I(E_k)$ through the energy conservation

$$E_k = h\nu - \Phi - E_B, \tag{2}$$

where Φ is the work function and E_B is the binding energy. Binding energies with occupied states thus result in high photoemission intensity at the corresponding photoelectron kinetic energy E_k. A higher photon energy $h\nu$ thus allows for a larger range of E_B to be probed. The first choice is thus for the range of binding energies that should be covered.

The second choice is for the desired probing depth. The electrons undergo inelastic scattering processes in their escape through the surface and the probing depth is governed by the inelastic mean free path (IMFP), which follows a remarkable universal curve[8]. The shortest IMFP of a few Å are found in the range of 20 eV $< E_k <$ 200 eV. Longer IMFPs up to several nm are found either at $E_k >$ 2000 eV or $E_k <$ 10 eV. For the study of valence electrons of low binding energy $E_B \sim 0$ we have $E_k \sim h\nu - \Phi$, thus the kinetic energy is governed by the photon energy and with typical $\Phi \sim$ 4–5 eV either photon energies above 2000 eV or below 15 eV would lead to reduced surface sensitivity, often a desired feature for solid state physics studies. We like to note, though, that in any case the outermost layers of the solid give rise to the highest intensities with an exponential suppression of the signal from the layers beneath. Thus in any case electron spectroscopy is a rather surface sensitive measurement.

Thirdly, the choice of photon energies affects the range of electron momenta that can be probed. Since the momentum component in the surface plane is conserved[9], one calculates readily

$$|\vec{k}_{||}| = \frac{1}{\hbar}\sqrt{2mE_k}\sin\theta, \tag{3}$$

where m is the free electron mass and θ is the emission angle measured from the surface normal. Assuming a free-electron model of the photoemission final state, we can even calculate the third momentum perpendicular to the surface as

$$k_\perp = \frac{1}{\hbar}\sqrt{2m(E_k\cos^2\theta + V_0)}, \tag{4}$$

where the inner potential V_0 is an adjustable parameter to account for the difference in reference potential inside and outside the solid[1]. The choice of photon energy is thus also influences the range of momentum that can be probed. Since we focus on $E_k \sim h\nu - \Phi$, in a given angular range, it is approximately proportional to $\sqrt{(E_k)} \sim \sqrt{(h\nu - \Phi)}$.

The fourth consideration concerns the quality of momentum space mapping. The conservation of $k_{||}$ (Eq. 3) holds universally for a well-ordered surface. Due to the high surface sensitivity, on the other hand, the ARPES experiment probes the near-surface region of the solid, where the momentum component $k_{||}$ is naturally perturbed by the broken translational symmetry perpendicular to the surface. The probing depth is governed by inelastic scattering and thus the effective resolution in $k_\perp$ is inverse proportional to the IMFP. Furthermore the free-electron final state model (Eq. 4) tends to be better applicable at larger kinetic energies due to reduced final state band structure effects[10]. The desire for accurate measurement of $k_\perp$ would thus be best fulfilled at higher photon energies.

The four choices above concern the properties of the photoemission process and the photoelectron. The fifth consideration has already been outlined in the introduction and concerns the energy resolution. This is fundamentally a property of the photon beam, as the total resolving power

$h\nu/\Delta E_{h\nu}$ of a grating monochromator is limited. The technological development leads to ever increasing numbers, though at a more-than-proportional expense of transmission of the monochromator. We consider a typical value as a respectable 20,000, with the highest number reported being 10^5[11]. For high energy resolution (low value of $\Delta E_{h\nu}$) a low photon energy $E_{h\nu}$ is thus the best choice. Also the properties of the electron spectrometer allow for best energy resolution at low electron kinetic energies, as the relevant ΔE_{ana} is governed by the analyser pass energy E_{P} in the energy dispersive element (hemispheres) besides geometrical factors. A low E_{P} corresponds to high energy resolution and for high E_{k} a strong retardation to E_{P} is thus required, complicating the design of the electron lens at the entrance of the analyser.

Taking these considerations together and aiming at an energy resolution ΔE_{comb} of 5 meV or better and a momentum range of a few $\mathrm{Å}^{-1}$ or larger, we identify an energy range of $h\nu = 20$–80 eV as the core operation range for high resolution ARPES. In this range the beamline resolution $\Delta E_{h\nu}$ can be kept well below 5 meV and the analyser resolution ΔE_{ana} can be readily matched to this. For this discussion we identify three further photon energy ranges extending the core range: (A) low energy of 8–20 eV: here a still higher energy resolution may be achieved and the low kinetic energy of the photoelectrons leads to a high momentum resolution at a given angular resolution according to by Eq. (3), which allows to resolve momentum structures in great detail[12] albeit in a limited momentum range. (B) extended ARPES range 100–300 eV: this range is useful for ARPES band mapping, namely Fermi surface mapping with better applicability of the free-electron-final-state approximation[10]. (C) higher photon energies $h\nu >$ 750 eV: these give access to core level excitations from all chemical elements.

The photon source of choice for a high flux monochromatic beamline is an undulator. The fundamental wavelength λ_1 emitted as from an undulator on axis is given by the undulator period λ_{u} and the K-value through

$$\lambda_1 = \frac{(1 + K^2/2)}{2\gamma^2}\lambda_{\mathrm{u}} \qquad (5)$$

(cited from Sect. 2-B2 of[13]), where the Lorentz factor $\gamma = E/(m_e c^2)$ is given by the storage ring energy E. The K-value parameterises the amount of excursion of the electron beam in the undulations and a larger K thus corresponds to a larger magnetic field strength on the electron beam axis. To lower the photon energy and thus increasing λ_1 an increased K is required, which is tuned by the undulator gap and the largest K available in a given undulator is limited by the minimum gap. In a storage ring with 3 GeV electron beam energy this undulator condition leads either to very long period λ_{u} of the undulator or a very large K-value at the lowest photon energy. The former choice leads to fewer undulator periods in a given device length (5 m in our case). The latter means that the criterion for an undulator of a moderate $K \leq 1$ is soon exceeded leading to emission of photons at energies far above the fundamental as well. Further considerations have to be made to ensure that the undulator can deliver all desired polarisations over the full photon energy range within the constraints of the minimum gap between the magnet banks, mechanical structure and magnet strengths.

We made the choice of a permanent magnet Apple-II undulator[14] with a period $\lambda_{\mathrm{u}} = 140$ mm, thus accommodating $n_{\mathrm{u}} = 34$ periods and two half-periods at the entrance and exit. The undulator delivers variable polarisation of linear horizontal and vertical and circular left and right with a mimimum gap of 23.5 mm down to a photon energy of 18 eV. At this energy our undulator is operated at a K-value of more than 8, which is considered more typical of a wiggler source, while it still generates an undulator-like photon beam for the fundamental energy. At this lowest gap it generates a total x-ray power of ≈4 kW and emits x-rays with photon energies up to ≈5 keV. This chosen undulator cannot deliver a beam for the extended range (A) of 8–18

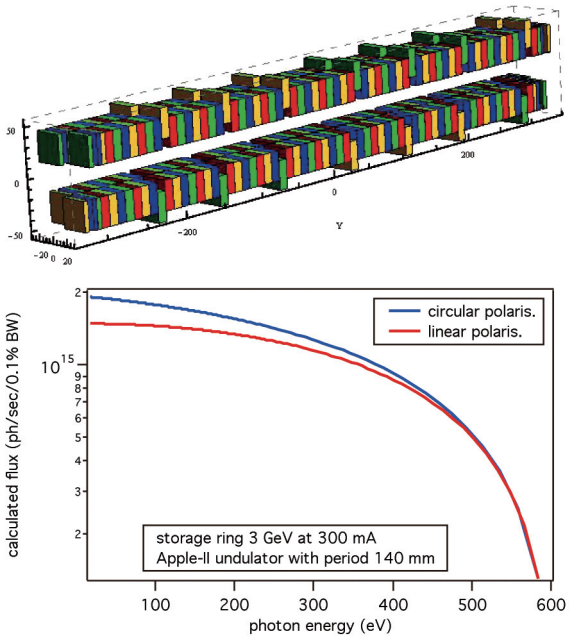

Fig. 1 (Color online) Schematic view of the 5 m long Apple-II undulator of beamline I05 and calculated flux of the fundamental emission line.

eV. When tuned to linear polarisation at $h\nu = 18$ eV it delivers about a quarter of the power into the beamline entrance aperture of 0.6×0.6 mrad^2, mostly rather high energy photons that are absorbed and not reflected off a mirror at a typical incidence angle of 3° in our case. At higher K it would deliver even higher power than the limit of 1 kW that was confirmed to be acceptable by careful design of the cooling system of the first mirror. The mirror will deform under the heat load, but the deformation can be kept low enough to allow for a sufficient optical performance of the beamline.

We have thus chosen an undulator that matches our identified core range. Implementing an Apple-II undulator for the extended range (A) at low photon energies, given by the heat load arguments above, would lead to reduced performance in the core range of 20–80 eV due to the combined effects of operation at lower K and less peak flux due to a lower n_u. Alternative undulator schemes based on the Figure-8 trajectory[15,16] or Knot trajectory[17] have been considered but rejected based on the limitation on available polarisations (only linear in case of Figure-8) and the still unproven design at the time of beamline design (for Apple-Knot or combinations of Figure-8 undulators) among other considerations. For the extended range (B), at photon energies up to 300 eV, the chosen undulator in our 3 GeV storage ring naturally delivers a very high flux on the fundamental, thus making this range naturally available. The extended range (C) of higher energies above 750 eV on the other hand, is covered already on the other dedicated photoemission beamline I09-SISA at Diamond Light Source and is no longer in the range of the fundamental of our undulator, thus the beamline does not delivery at such high photon energies although a careful tuning on a higher (quasi-) harmonic of the undulator may deliver a beam with just sufficient intensity for some photoemission core level characterisations of samples as well.

The higher harmonic contamination of the beam is a further serious issue that needs to be addressed. The grating monochromator will not provide much in the way of higher harmonic rejection and absorption filters are equally difficult to implement, strongly reducing the total photon flux. Higher harmonics in the photon beam affect the photoemission spectra by exciting photoelectrons at the higher energies. These are emitted, like the photoelectrons from the fundamental, as elastic emission peaks and also a broad spectrum of inelastically scattered and secondary electrons. With the electron spectrometer tuned to emission on the fundamental at lower energy, these photoelectrons excited at higher energy will give at best a constant background, thus reducing signal-to-noise, at worst they will give spurious peaks of intensity in the spectra. This is of particular concern for the second harmonic (twice the photon energy) in the case of resonant photoemission, where the photon energy is tuned over a range in the vicinity of the binding energy of a core level in question. The strong peak of core level emission from the second harmonic falls into the range of spectrum that corresponds to low binding energies with respect to the fundamental. We have chosen to address this problem at the source by introducing a strong phase error into the undulator that reduces the intensity of higher harmonics by shifting their photon energy to peaks that lie away from the precise multiple of the fundamental and thus filtering out these photons in the fully harmonic monochromator. This phase error is achieved by a quasi-harmonic scheme[18], though with very few of the magnet blocks modified not to perturb the basic periodicity of the undulator too much. A full simulation of all properties of the source by calculations now becomes a formidable task requiring the tuning of the gap to make full use of the 0.6×0.6 mrad^2 entrance aperture of the beamline, at each gap setting and considering all four cases of polarisations, where the movements of magnet banks of the Apple-II structure shift the modified magnet blocks to new positions. We have thus chosen to optimise the quasi-periodic scheme of the undulator only considering the lowest photon energy case of $h\nu = 18$ eV and with the criteria that we will reduce the peak flux of the fundamental into the beamline entrance aperture by no more than 20% and aiming to get the highest reduction of the second harmonic (twice the photon energy of the fundamental) in particular for all four cases of polarisation. This optimisation was performed by Dr. Emily Longhi of Diamond Light Source and the undulator was built, installed and commissioned by the expert team of the Insertion Devices group under the leadership of Dr. Jos Schouten.

From this source the natural choice of monochromator is an entrance slit-free grating monochromator with a vertical dispersive plane. Due to its wide application on other Diamond beamlines and its excellent track record of delivering high resolution[11], we have chosen the collimated beam plane grating monochromator (PGM). Besides the grating and exit slit, this scheme consists of a plane mirror and two curved mirrors. The grating and plane mirror use variable incidence angles that are calculated according to the grating equation [13, Sect. 3.4]. A toriodal first mirror (collimating mirror CM) and a cylindrical mirror after the grating (focussing mirror FM) focus the beam onto the exit slit, which selects the photon energy. The exit slit as well

as the intermediary horizontal beam waist are re-focussed after the exit slit by a refocussing mirror (RFM). The scheme thus consists of four mirrors and the grating, the latter is exchangeable in-situ by moving the grating holder assembly laterally. A similar scheme employing a variable line-spacing grating (VLS) could deliver equivalent performance with one mirror less, thus facilitating alignment. With the two-branch scheme we opted to use two different FMs on a common mechanical holder to switch the beam into either of the two branches and focus onto either of the two branchline exit slits.

Having chosen the source and the monochromator scheme, we can now optimise the beamline optics to deal with the heat load generated, mostly by photons of energy much higher than the fundamental. Of particular concern is the first mirror CM. With the highly variable heat load, a cryogenic operation around 120 K, the zero expansion point of silicon, requires careful engineering of a variable power counter heater against a high power cryo-cooler. Cooling by water at room temperature, on the other hand, readily provides the required cooling power and works by a less sophisticated coolant distribution system that flows the water through cooling brackets on either side of the mirror. With this choice a balanced design of the cooling brackets, the contact surfaces and the cross-sectional shape of the silicon block (length 250 mm) is required, to counter the effects of a heat bump and of bending of the silicon block due to the temperature difference between the front and the back. By detailed finite element calculations a design was achieved that allows the back of the mirror to remain warmer than the cooling water temperature at high heat load operation, thus reducing the bending effect and still providing high cooling power to avoid a strong heat bump. The latter is furthermore kept uniform by illuminating, in terms of heat load, the whole length of the mirror. Calculations showed us that an alternative internally cooled silicon mirror might performs better for the vertical collimation property due to its smaller heat bump but the side cooled scheme performs better in the horizontal focussing plane. Its performance in the vertical plane, which is the dispersive plane of the grating is good enough, in particular since the deterioration of performance occurs only at low photon energies, where the unperturbed resolving power naturally goes up and easily exceeds values of 20,000. For the second mirror, which is the plane mirror in the PGM, the internally cooled scheme was chosen. Due to the variable incidence position of the beam on this mirror the flexibility of providing cooling just where it is needed adds to the benefit of absence of distortions due to the clamping of brackets onto this long mirror (400 mm). The evaluation of this detailed balance design was carried out by Dr. Hongchang Wang in the Optics Group of Diamond under the leadership of Dr. Kawal Sawhney.

The choice of our core photon energy range of $h\nu = 20$–80 eV as well as the requirement of stability under high heat load now lead naturally to the choice of coating for the mirrors. In this range the reflectivity of high density carbon reaches high values well above 90% of reflectivity at the chosen incidence angle of 3°, with a smooth energy dependence over the full range. Other metallic coatings may give higher reflectivities at particularly favourable wavelengths but lower overall reflectivity. High quality coatings of diamond-like-carbon at suitable densities exceeding the one of graphite are readily available from various suppliers. Only the gratings could not be coated with this method, as the groove edges may be rounded. The most prominent disadvantage of the carbon coating consists of a large dip of reflectivity around 300 eV due to the K-edge absorption of carbon. Our beamline thus cannot deliver any significant photon flux in the range of approx. 240–400 eV. This disadvantage may be offset by the long term stability of the mirrors, as any contamination is likely to contain carbon as well, and the effects of a contamination film on the high density carbon will be less severe than on a metallic coating.

The detailed optical scheme, including mirror deflection angles and positions can now be developed. The final optimised focussing scheme is summarised in **Fig. 2**. We have

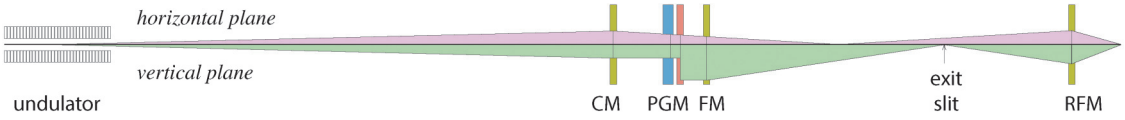

Fig. 2 (Color online) Schematic diagram of the monochromator and focussing optics of the HR-branch. The top half represents the horizontal plane with the beam envelope shown in red and the bottom half the vertical plane shown in green. Horizontally deflecting mirrors (CM, FM and RFM) are shown in yellow, the vertically deflecting plane mirror and grating are shown in blue and red, respectively. The latter two form the PGM. The asymmetric scattering geometry of the grating in first order internal diffraction condition leads to an effective increase in the beam profile (anamorphic magnification), shown as an increased size of collimated beam in the vertical plane.

benefit from the availability of space for a long beamline, and a focal length of FM of 11 m was chosen, bringing the total dispersion length from grating to exit slit of more than 12 m. A subtle balancing was required for the position of the horizontal intermediary focus, generated by CM and thus common to both branches, which we placed 6 m after the FMs. On the nano-branch of the beamline the FM has a focal length of 6 m, thus bringing the horizontal and vertical focus (exit slit) together (stigmatic). This makes the intermediary focus of the HR-branch astigmatic with an RFM that demagnifies by a factor of three in the vertical and by 5.5 in the horizontal (geometric demagnification factors). An elliptical mirror shape is required for this high demagnification and the final mirror shape of the refocussing mirror is an elliptical torus. The focussing mirrors CM, FM and RFM all utilise a pre-set incidence angle of 3° and are placed on hexapod mechanical holders providing high flexibility and precise, reproducible positioning adjustments.

A final consideration has to be made for the desired spot size on the sample. This needs to be small enough to be able to measure typical small regions of homogeneous sample within a cleavage surface, which can be as small as 100 $\times$ 100 μm, but an excessively small spot may provide too high flux density leading to space charge-induced deterioration of the energy resolution. The detailed results of the optics design and final performance will be reported in a separate publication.

The optics design was performed in consideration of the available floor space. The final floor space arrangement is shown in **Fig. 3**. The individual rooms of the beamline enclosure are (i) a lead shielded hutch for mirror CM and heat load selecting water-cooled slit units, (ii) an optics room for the PGM, the mount of the two FMs and the two exit slits for the two branches, (iii and iv) two end station rooms for HR-ARPES and nano-ARPES, (v) a control room and (vi) a sample preparation room. Each room has good temperature insulation against the other rooms and the beamline perimeter and individual temperature stabilisation to less than 0.1℃ over a typical week. The end station equipment nano-ARPES is shown in grey as the design was not finalised at the time of producing the graphics and will be described in a separate publication.

III. CHOICES FOR END STATION

The choices for constructing a high-resolution ARPES end station start with the choice of electron analyser. Hemispherical analysers of exceptional quality are commercially available from several suppliers. The angle-multiplexing lens and hemispherical field dispersive element arrange the photoelectrons onto the detector plane with a range of kinetic energies in one direction and positions along the entrance slit, corresponding to different emission angles, along the other. Sweeps of the retard voltage that decelerates the photoelectrons from their initial kinetic energy E_k to the pass energy E_P in the hemispheres allow for the the acquisition of extended ranges of kinetic energies. We chose to have a grid-free detector, which proved to give excellent performance despite the potentially reduced quality of field termination and suppression of electrons that are inelastically scattered from the walls of the hemispheres. With this detector we can acquire data of high quality in static mode, *i.e.* without sweeping the retard voltage. For typical energy ranges of interest, this reduces the acquisition time needed to accumulate a certain number of counts by approximately a factor of two.

Much higher flexibility lies in the choices for a sample manipulator. This forms the sample environment (temperature) during the measurement and is often also used for some aspect of surface preparation. We consider that the

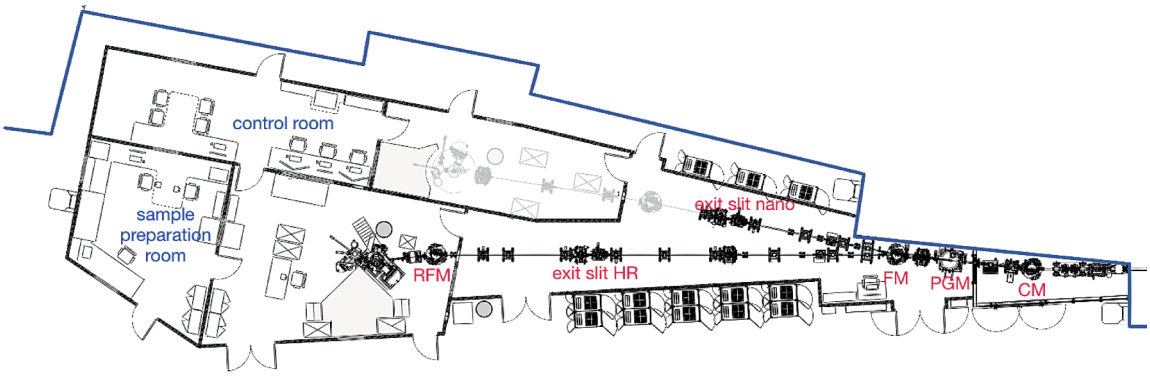

Fig. 3 (Color online) Floor plan of the beamline installation I05 with rooms for optics, end stations, sample preparations and a control room. The main mirror locations are shown as CM, PGM, FM, and RFM as explained in the text.

most important for a successful ARPES experiment are the three following aspects: (a) ability to go to low temperatures (<10 K) reliably and easy adjustment of the sample temperature, (b) precise and reproducible positioning to direct the beam to a small spot on the sample under investigation and (c) full angular rotation flexibility for mapping of full angular cones by rotation of the sample with respect to the photon polarisations, electron lens axis and entrance slit into the hemispheres. To achieve these objectives, we have purchased a commercial Helium flow cryostat that forms a vacuum cold finger as well as a commercial positioning table including a rotation stage for rotation around the cryostat main axis.

We have constructed a goniometry head that allows for a tilt motion over an range of +45 to −30° and, internal to this, an azimuth rotation with range ±120°. The mechanical sample support is independent of the cryostat, which is attached to the sample holding block by a braid. This Cu block and braid are kept light weight for fast thermalisation. The goniometer gears and a Cu sheet metal shell around them are cooled by the exhaust helium in the backflow of the cryostat to provide a thermal shield, but the longest part of the mechanical support is held at room temperature to keep the change of sample position due to thermal contraction at less than 300 μm from room temperature to the lowest measurement temperature of 7 K.

The most frequently used sample preparation method is in-vacuum cleavage of single crystals at cryogenic temperatures to expose a fresh surface. These surface can be further modified by adsorption of additional atoms, mainly alkali metals Li, Na, K, Rb or Cs, at small coverages. This is particularly useful in the case of semiconductors and materials close to a metal-to-insulator transition where the electron transfer from the adsorbate can lead to additional states becoming occupied and thus observable in ARPES and the transition itself may be fine-tuned. In the case of oxides the irradiation during the measurement itself can often lead to a modification of the surface. For oxides this can be countered by exposure to molecular or atomic oxygen. We have opted not to do any of these treatments in the measurement position as they might damage the analyser, but we have arranged for alkali metal evaporations, as well as atomic oxygen treatment from a gas cracker device to be performed in the position where the sample is retracted away. The treatment can thus be applied to the cryogenically cold sample and then the measurement position is quickly restored by moving the manipulator back to the measurement location. More sophisticated preparations, such as sputter and anneal cycles of metal surfaces and very high temperature heating up to 1000℃ are performed by removing the sample from the main manipulator and attaching it to a high temperature manipulator in the adjacent Interface Chamber (IC) vacuum chamber, where also small amounts of other materials, such as Si or Te, can be deposited by evaporation deposition.

The full configuration of vacuum chambers of the HR-ARPES is shown in **Fig. 4**. The transfer between one chamber and another is performed by grabbing the sample holder by its handle with an ultrahigh vacuum grabber attached to a magnetically coupled transfer arm. Each chamber thus needs to contain one or several recipient positions where the sample plates can slide into and are detached from the transfer arm. These positions include the manipulators, but also multi-position devices to store samples. The

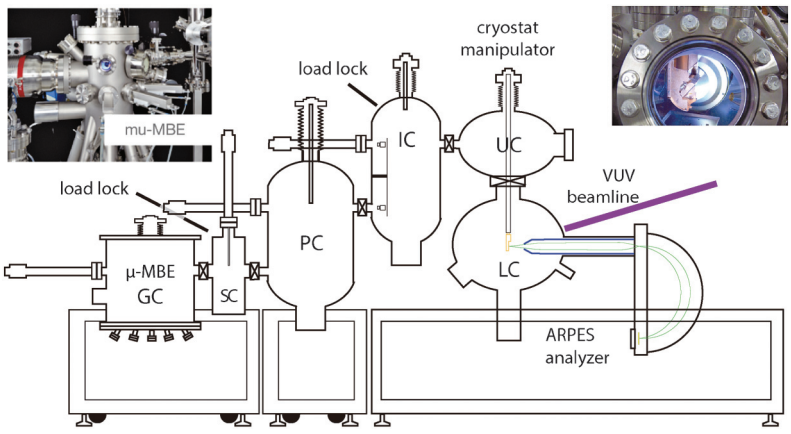

Fig. 4 (Color online) Schematic view of various vacuum chambers of the HR-ARPES end station, consisting of the analysis chambers upper and lower chamber (UC and LC), the interface chamber (IC) the preparation chamber (PC), the storage chamber (SC), the MBE growth chamber (μ-MBE or GC) and two load locks. The insert photos show the μ-MBE sample growth facility on the left and a view of the main cryogenic sample manipulator on the right.

main load lock attached to the IC also contains a multi-position recipient, this time itself attached to a transfer arm. This chamber is vented to atmospheric pressure by admission of dry N_2 gas and then pumped down quickly after inserting samples. The pressure achieved here is 5×10^{-8} mbar after a few hours, when the gate valve to the IC at base pressure of 1×10^{-10} mbar or lower may be opened. The IC thus acts as the second stage of a two-stage load lock and it was an important design consideration not to attach a load lock directly to a chamber containing a cryogenic manipulator as the water and other contaminations that are inevitably introduced by the loading procedure would cryo-sorb on the cold surfaces and then lead to unacceptable degassing and contamination of the sample surface as soon as the sample temperature is raised.

IV. SAMPLE PREPARATION FACILITIES

The IC, UC and LC chambers are optimised for the preparation and measurement of cleaved single crystal surfaces by the multi-position load lock and efficient transfers. More complicated surface preparations can be performed in the PC, SC and μ-MBE parts of the system. The μ-MBE derived its name from the very compact design, optimised for highly reproducible molecular beam epitaxy (MBE) from effusion cells including complicated oxide and co-evaporation sample preparations. The system has been described in Ref.[19]. The focus lies on materials growth on various substrates at film thicknesses that are often thick enough to be considered as bulk-like in ARPES, but with the additional benefit of being able to introduce strain into the materials due to lattice mismatch between the substrate and the film. The MBE technique then also allows to reduce the film thickness to the ultra-thin limit.

The μ-MBE is complemented by the surface characterisation and preparation chamber PC. Here the sample properties can be examined by X-ray Photoelectron Spectroscopy (XPS) using an unmonochromatised twin-anode x-ray source and an additional small hemispherical analyser and by low-energy electron diffraction (LEED). Additional MBE evaporator ports can be used, especially for very low deposition rates and ultrathin films, where the film growth can be monitored in real time by running XPS data acquisitions in the same position where depositions are performed by recording the intensity of corresponding peaks, representative of the atomic species. In the case of suitable substrates (*e.g.* metal single crystal surfaces) a fresh surface can be prepared by Ar ion sputtering and subsequent annealing with a heater up to 600℃ integrated in the PC manipulator. Then a new film can be deposited.

Sample preparations by these well-established surface preparation methods compete for sample quality with the cleaved single crystals. Furthermore the full sample characterisation has to be performed in the vacuum system of the beamline end station as any exposure to air usually modifies the sample properties. Thus the beamline users do well to calibrate procedures and evaporation rates well before the beamtime and establish the best growth recipe before the first attempt to observe ARPES data as well as acquiring as many characterisation data as possible. This is achieved by allocating a dedicated floor space and operator desk to the PC/SC/μ-MBE combination and detaching it from the IC, except for a soft bellows vacuum connection through which the grown samples can be transferred. In this way two independent teams can work on the end station instrument in parallel, one acquiring ARPES data from (usually cleaved) samples and the other optimising their sample preparations for the upcoming beam time.

V. PERFORMANCE

The performance of the beamline is best judged by its impact on the scientific community as measured by the publication record of the beamline users[20]. These benefit from the high flux of photons, easily tuneable in photon energy and polarisation, while being able to set a high energy resolution of $\Delta E_{\mathrm{comb}} < 2$ meV as well. At relaxed resolution, the acquisition times are usually limited only by the restriction in illumination intensity of the detector, which needs to be kept low enough to minimise the performance reduction of the multichannelplate electron amplifier. The data acquisitions are also made highly efficient through the use of a fast integrated control and detector read-out system, that allow setting the undulator, the monochromator, the sample manipulator and the analyser from within one single data acquisition system and performing highly flexible scans of all components.

Furthermore the ease of sample transfer and positioning allow for a rapid succession of samples to be measured (up to one sample cleavage per hour), which is particularly important when the cleaves are unsuccessful and an assessment of the data during alignment allows for quick decisions on changing sample to the next cleavage attempt. Once successfully cleaved the samples are kept stable over long times due to low residual gas levels thus reducing unwanted surface adsorption.

VI. DISCUSSION AND OUTLOOK

The beamline performance cannot be cast into a single number and the concerted optimisation of all parameters

was enabled through the use of proven technology and numerical simulation calculations. The combined experience of other similar installation has informed the design decisions and optimisations. Therefore, it should be expected that the a next generation of a similar beamline project will set slightly different priorities and arrive at still better results by incorporating the experience gained on the current facilities.

The high productivity currently arises from the efficient preparation of fresh surface by cleavage of interesting materials. The last decade or two have seen multiple discoveries of new classes of materials (high T_c oxide superconductors, Graphene, iron based superconductors, topological insulators and Dirac and Weyl semimetals to name a few). While it is sometimes felt that the last easily cleavable sample will soon have been measured, it is equally conceivable that a new wave will emerge soon. In this case a beamline should be ready to accommodate the ARPES measurement from this new samples, ideally on a similar time scale after successful synthesis where also the resistivity and atomic structure are determined. Furthermore the modification of surfaces by controlled adsorption or occasionally by desorption, *e.g.* under irradiation, will continue to play an important role in the rapid characterisation of the electronic structure materials by ARPES.

Some materials and ultrathin film systems, however, cannot be produced by synthesis and cleavage. These need to be grown *in-situ* in the same vacuum system where measurements are performed to arrive at a chemically well defined and well-ordered surface that can be measured by ARPES. Here the development cycles are much slower as growth equipment (evaporators) needs to be attached and calibrated and growth recipes need to be refined. This process may be accelerated by performing growth in separate installations and then introducing samples into the ARPES instrument by a vacuum suitcase transfer. We think that *in-situ* growth offers exciting opportunities to get data from materials that are otherwise not ''ARPESable'' and to create unique ultrathin film structures.

For the development of the beam technology, the energy resolution will continue to increase at still high enough photon flux to make a useful beam. This needs to be complemented by still further reduced measurement temperatures and make use of the best electron spectroscopy equipment. As a second priority, the desirable photon energy range is under constant review. Expansion of the range to higher photon energies, up to 800 or 1000 eV would often be desirable, especially if the energy resolution can be kept below about 20 meV (resolving power 40,000 to 50,000). Other installations that have aimed to cover the full range from 20–800 eV have, however, usually homed in on a reduced range that is then effectively used for experiments. The necessary design changes for photon energies below 12 eV are much harder to achieve on a 3 GeV storage ring. This range is already well covered by laser sources, albeit at a small selection of fixed photon energies. Synchrotron radiation offers the much easier tuneability[15], which is an important feature as the precise photoemission conditions can change very rapidly and a full optimisation can only be done by experimental adjustments and trials.

In conclusion, we are convinced that the construction of an ARPES facility was a good choice for a national facility, such as Diamond Light Source, serving both national and international users. With attention to detail it was possible to tune the facility to fairly high throughput and thus open the technique, with some training effort required, also to users who have little previous ARPES experience but who have interesting samples and interesting questions to address. ARPES, a mature technique, continues to provide unique and very useful data about the samples under study and thus will continue to play an important role in the investigation of the electronic structure of solids and their surfaces. Our beamline, including both the HR-branch described here as well as the newer nano-branch is open to application for beamtime to user from around the world[21].

VII. ACKNOWLEDGEMENTS

This beamline design and construction project has benefit from discussions with uncountable academic colleagues and engineers, technicians as well as administrative staff in all departments of Diamond Light Source as well as the multiple supplier companies of specialised equipment have all contributed significantly to the success of the project. We wish to acknowledge in particular Professors Colin Norris, Gerd Materlik, Richard Walker and Trevor Rayment of the senior management team of Diamond Light Source for their untiring efforts in preparing the project, through approval, and their continued efforts of organising and supporting the project. Their leadership has played an important role in arriving at the decisions that have been described in this article.

Reference

1) S. Hufner, ed.: *Very High Resolution Photoelectron Spectroscopy* (Springer, 2007).
2) A. Damascelli: Phys. Scr. **T109**, 61 (2004).
3) M. R. J. C. Campuzano, M. R. Norman: *Photoemission in the High Tc Superconductors* (Springer, Berlin, 2004), vol. II of

Physics of Superconductors, pp. 167–273.
4) F. Reinert and S. Hüfner: New J. Phys. **7**, 97 (2005).
5) T. Shimojima, K. Okazaki and S. Shin: J. Phys. Soc. Jap **84**, 072001 (2015).
6) X. Zhou, B. Wannberg, W. Yang, V. Brouet, Z. Sun, J. Douglas, D. Dessau, Z. Hussain and Z.-X. Shen: J. Electron Spectrosc. Relat. Phenom. **142**, 27 (2005).
7) S. Hellmann, K. Rossnagel, M. Marczynski-Bühlow and L. Kipp: Phys. Rev. B **79**, 035402 (2009).
8) M. P. Seah and W. A. Dench: Surf. Interface Anal. **1**, 2 (1979).
9) J. Pendry: Surf. Sci. **57**, 679 (1976).
10) V. Strocov: J. Electron Spectrosc. Relat. Phenom. **130**, 65 (2003).
11) M. Weiss, R. Follath, K. Sawhney, F. Senf, J. Bahrdt, W. Frentrup, A. Gaupp, S. Sasaki, M. Scheer, H.-C. Mertins *et al.*: Nucl. Instrum. Methods in Physics Research Section A: Accelerators, Spectrometers, Detectors and Associated Equipment **467**, 449 (2001).
12) A. Tamai, W. Meevasana, P. D. C. King, C. W. Nicholson, A. de la Torre, E. Rozbicki and F. Baumberger: Phys. Rev. B **87**, 075113 (2013).
13) A. C. Thompson, D. T. Attwood, E. M. Gullikson, M. R. Howells, J. B. Kortright, A. L. Robinson, J. H. Underwood, K.-J. Kim, J. Kirz, I. Lindau *et al.*, *X-ray data booklet*, Lawrence Berkeley National Laboratory, University of California, Berkeley, California 94720 (2009).
14) S. Sasaki: Nucl. Instrum. Methods in Physics Research Section A: Accelerators, Spectrometers, Detectors and Associated Equipment **347**, 83 (1994).
15) P. Vilmercati, M. Barnaba, L. Petaccia, A. Bianco, D. Cocco, C. Masciovecchio and A. Goldoni: Notiziario Neutroni e Luce di Sincrotrone **13**, 25 (2008).
16) S. Yamamoto, Y. Senba, T. Tanaka, H. Ohashi, T. Hirono, H. Kimura, M. Fujisawa, J. Miyawaki, A. Harasawa, T. Seike *et al.*, J. Synchrotron Rad. **21**, 352 (2014).
17) F. Ji, R. Chang, Q. Zhou, W. Zhang, M. Ye, S. Sasaki and S. Qiao: J. Synchrotron Rad. **22**, 901 (2015).
18) S. Sasaki, H. Kobayashi, M. Takao, Y. Miyahara and S. Hashimoto: Rev. Sci. Instrum. **66**, 1953 (1995).
19) A. A. Baker, W. Braun, G. Gassler, S. Rembold, A. Fischer and T. Hesjedal: Rev. Sci. Instrum. **86**, 043901 (2015).
20) *Website of beamline* I05 –ARPES, *see section on publications*, http://www.diamond.ac.uk/I05.
21) *Website with information on application for beamtime at diamond light source*, http://www.diamond.ac.uk/Users.html.